BUNDLE BLOCK ADJUSTMENT OF OMNI-DIRECTIONAL IMAGES OBTAINED FROM A GROUND MOBILE MAPPING SYSTEM

T. Oh [a], K. Choi [a], I. Lee [a], *

[a] Department of Geoinfomatics, The University of Seoul, 90 Jeonnong-dong, Dongdeamun-gu, Seoul 130-743, Korea
- (theidps, shale, iplee)@uos.ac.kr

Commission I, WG I/3

KEY WORDS: Omni-Directional Camera, Ground Mobile Mapping System, Bundle Block Adjustment, GPS/INS, Multi-sensors

ABSTRACT:

Regarding the increasing demands for high quality spatial information, many researchers have emphasized the need for multi-sensor/platform integration for more rapid and economical generation of such spatial data. Most systems employing a set of frame cameras may have suffered from their small fields of view and poor base-distance ratio. These limitations can be significantly improved by employing an omni-directional camera that is capable of acquiring images in every direction. Using a GMMS integrated with this camera, we can enlarge the mapping coverage and observe objects from a variety of directions and positions. Bundle Block Adjustment (BBA) is one of the existing georeferencing methods to determine the exterior orientation parameters of two or more images. In this study, by expanding the concept of the traditional BBA method, we attempt to develop a mathematical model of BBA for omni-directional images with GPS/INS data and Ground Control Points (GCPs). The proposed mathematical model includes two main parts; observation equations based on the collinearity equations newly derived for omni-directional images and stochastic constraints imposed from GPS/INS data and GCPs. We also report the experimental results from the application of our proposed BBA to the real data obtained mainly in urban areas. With the different combinations of the constraints, we applied four slightly different types of mathematical models. The type where only GCPs are used as the constraints provides the most accurate results, less than 5 cm of RMSE in the estimated ground point coordinates. In future, we plan to perform more sophisticated lens calibration for the omni-directional camera to improve the georeferencing accuracy of omni-directional images. These georeferenced omni-directional images can be effectively utilized for city modelling, particularly autonomous texture mapping for realistic street view.

1. INTRODUCTION

As the demand for high quality spatial information such as sophisticated 3D city model are being increased, many researchers have attempted multi-sensor/platform integration to obtain spatial data more rapidly and economically. One of the most promising systems to acquire spatial information along roads is a Ground Mobile Mapping System (GMMS) usually equipped with imaging cameras, laser scanners, and GPS/INS (Gontran, 2003; Vincent, 2005).

Most systems employing a set of single frame cameras may have problems due to limited Field Of View (FOV) and poor base-distance ratio. These problems can be substantially solved by incorporating an omni-directional camera which can acquire an omni-directional field of view at a time without any movement or rotation of the camera (Aizawa, 2004).

Using a GMMS with this camera, we can observe objects from almost entire directions. Such capability allows us to generate more complete and realistic street view. In past, most omni-directional cameras utilize spherical mirrors with a single detector, inherently retaining significant level of distortions (Silpa, 2005). Many researchers should attempt to remove or reduce such distortions (Beauchemin, 2001).

Later some recent omni-directional cameras such as Ladybug (Point Grey Research, 2008) are integrated with a set of single frame cameras and generate a large image showing scenes in all directions by stitching each image together. Such a camera can generally obtain high resolution omni-directional images with small distortions, which may be also useful for 3D precision mapping of road-side objects. The mapping process requires accurately georeferenced omni-directional images.

Georeferencing is a process to determine the exterior orientation parameters of images, that is, the position and attitude of the camera at the time of exposure for each image (Choi, 2009). One of the most popular georeferencing methods is Bundle Block Adjustment (BBA), where we can estimate exterior orientation parameters and ground point coordinates by adjusting the light bundles originating from image points.

Traditionally, the BBA method has been defined for a set of frame camera images and intensively used for 2D or 3D mapping from these images. To apply this well-established method to omni-directional images rather than frame camera images, we have to modify its mathematical models. Hence, in this study, we attempt to develop the mathematical models of BBA for omni-directional images with GPS/INS data and GCPs.

The proposed mathematical model is derived through two steps. First, we derive new collinearity equations for omni-directional images, representing the geometric relationships between a ground point and the corresponding image point on an omni-directional image. A set of observation equations based on these collinearity equations are then established. Second, from GPS/INS data and GCPs, we formulate two kinds of stochastic constraints for BBA. Based on these two step derivation results, we finally present four different models according to the selection of different unknowns and constraints.

---

* Corresponding author.

2. METHODOLOGY

2.1 Overview

As the main input, the proposed BBA method requires tie points (TPs) manually or automatically selected from omni-directional images. In addition, to overcome the datum deficiency, it also uses GPS/INS data and (or) GCPs. With these inputs, as like the traditional BBA methods, the proposed method is also to estimate the EOPs of each omni-directional image and GPs (Ground Points) corresponding to all the TPs.

The mathematical models for the proposed BBA method consists of two main parts. The first one is the observation equations associated with TPs, expressed as Eq. (1). The second one is the stochastic constraints associated with GPS/INS data and GCPs, expressed as Eq. (2) and (3), respectively.

A. Observations: $\quad Y = F(\Xi_E, \Xi_P) + e_y \quad$ (1)
B. Constraints: $\quad Z_1 = G_1(\Xi_E) + e_{z1} \quad$ (2)
$\quad\quad\quad\quad\quad\quad Z_2 = G_2(\Xi_P) + e_{z2} \quad$ (3)

where
$\quad Y$ = observations derived from TPs
$\quad Z_1$ = constraints derived from GPS/INS data
$\quad Z_2$ = constraints derived from GCPs
$\quad e_y$ = the measurement errors associated with Y
$\quad e_{z1}$ = the measurement errors associated with Z_1
$\quad e_{z2}$ = the measurement errors associated with Z_2
$\quad \Xi_E$ = unknowns for EOPs
$\quad \Xi_P$ = unknowns for GPs

The observation equations are based on the new collinearity equations associated with an omni-directional images rather than ordinary frame camera images. GPS/INS data and GCPs are used as the stochastic constraints for EOP and GPs, respectively. More detail derivations in both parts are presented in the following sections.

2.2 Observation Equations based on Collinearity Equations

The collinearity equations indicate the relationship between ground points and image points. An ordinary frame camera generates an image through the perspective projection of a 3D scene to a 2D focal plane. However, an omni-directional camera generates an image through the perspective (central) projection to 3D spherical surface. Therefore, we should derive new collinearity equations for omni-directional images with some modifications to the existing equations.

Let assume that ^{G}P is the coordinate vector of a ground point expressed in a ground coordinate system (GCS). This point can be expressed as ^{G}P in the camera coordinate system (CCS) using the coordinate transformation in Eq. (4). Here, $^{G}O_C$ is the origin of CCS expressed in GCS and $^{C}_{G}R$ is a rotation matrix from GCS to CCS.

$$ ^{C}P = {}^{C}_{G}R({}^{G}P - {}^{G}O_C) \quad (4) $$

The ground point is then projected to a spherical surface toward the projection center, that is, the origin of CCS, as shown in Figure 1. The projected image point ρ can be expressed with a horizontal angle (α) and a vertical angle (β). These angles are expressed as Eq. (5), where $^{C}P_x$, $^{C}P_y$ and $^{C}P_z$ indicate the 3D coordinates of ^{C}P.
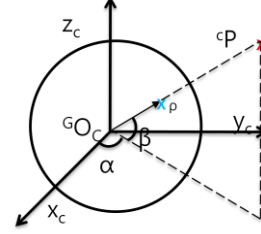

Figure 1. Central projection of GP to a spherical surface

$$ \rho = \begin{bmatrix} \alpha \\ \beta \end{bmatrix} = \begin{bmatrix} \text{atan2}({}^{C}P_y, {}^{C}P_x) \\ \text{asin}({}^{C}P_z/||{}^{C}P||) \end{bmatrix} \quad (5) $$

By combining Eq. (4) and (5), we can express the relationship between a GP (^{G}P) and the corresponding image point (ρ) on an omni-directional image with its EOP of $^{C}_{G}R$ and $^{G}O_C$. The combined equations indicate the collinearity equations for omni-directional images.

Based on the collinearity equations, the observation equations for an image point can be expressed as Eq. (6), where σ_0^2 is the variance of the image point measurement errors and I_2 is 2 by 2 identity matrix. The equations actually involves nine parameters, the ground point $^{G}P = ({}^{G}P_x, {}^{G}P_y, {}^{G}P_z)$, the projection center $^{G}O_C = (X_C, Y_C, Z_C)$, and the rotational angles (ω, ϕ, κ) for $^{C}_{G}R$.

$$ \rho = \begin{bmatrix} \alpha \\ \beta \end{bmatrix} = \begin{bmatrix} \text{atan2}({}^{C}P_y, {}^{C}P_x) \\ \text{asin}({}^{C}P_z/||{}^{C}P||) \end{bmatrix} + e, e \sim (0, \sigma_0^2 I_2) \quad (6) $$

The nonlinear equations in Eq. (6) can be linearized into Eq. (7) using a Taylor series. Here, Ξ is the vector of nine parameters, Ξ_0 is its initial approximation; and f is the functions for the collinearity equations.

$$ \rho \simeq f(\Xi_0) + \partial f/\partial\Xi \mid_{\Xi=\Xi_0} (\Xi - \Xi_0) + e, e \sim (0, \sigma_0^2 I_2) \quad (7) $$

We can express the Jacobian matrix in Eq. (7) as

$$ \frac{\partial F}{\partial \Xi} = \begin{bmatrix} \frac{\partial f_1}{\partial \Xi} \\ \frac{\partial f_2}{\partial \Xi} \end{bmatrix} = \begin{bmatrix} \frac{\partial \text{atan}(t_1)}{\partial t_1} & \frac{\partial t_1}{\partial \Xi} \\ \frac{\partial \text{asin}(t_2)}{\partial t_{12}} & \frac{\partial t_2}{\partial \Xi} \end{bmatrix} = \begin{bmatrix} \frac{\partial \text{atan}(t_1)}{\partial t_1} & \frac{\partial t_1}{\partial {}^{C}P} \\ \frac{\partial \text{asin}(t_2)}{\partial t_{12}} & \frac{\partial t_2}{\partial {}^{C}P} \end{bmatrix} \frac{\partial {}^{C}P}{\partial \Xi}. \quad (8) $$

where

$$ \begin{bmatrix} t_1 \\ t_2 \end{bmatrix} \equiv \begin{bmatrix} {}^{C}P_y/{}^{C}P_x \\ {}^{C}P_z/\|{}^{C}P\| \end{bmatrix} \quad (9) $$

The partial differentiation in Eq.(8) is expressed as

$$\begin{bmatrix} \dfrac{\partial \operatorname{atan}(t_1)}{\partial t_1} \\[2mm] \dfrac{\partial \operatorname{asin}(t_2)}{\partial t_2} \end{bmatrix} = \begin{bmatrix} \dfrac{1}{1+(t_1)^2} \\[2mm] \dfrac{1}{\sqrt{1-(t_1)^2}} \end{bmatrix} \tag{10}$$

$$\frac{\partial}{\partial {}^C P}\begin{bmatrix} t_1 \\ t_2 \end{bmatrix} = \frac{\partial}{\partial {}^C P}\begin{bmatrix} \frac{{}^C P_y}{{}^C P_x} \\[2mm] \frac{{}^C P_z}{\|{}^C P\|} \end{bmatrix} = \begin{bmatrix} -\frac{{}^C P_y}{{}^C P_x{}^2} & \frac{1}{{}^C P_x} & 0 \\[2mm] -\frac{{}^C P_x {}^C P_z}{\|{}^C P\|^3} & -\frac{{}^C P_y {}^C P_z}{\|{}^C P\|^3} & \frac{{}^C P_x{}^2 + {}^C P_y{}^2}{\|{}^C P\|^3} \end{bmatrix} \tag{11}$$

Finally, $\frac{\partial {}^C P}{\partial \Xi}$ can be rewritten as Eq. (12) where Ξ_1 is GP coordinates, Ξ_2 is the camera position parameters; and Ξ_3 is the camera attitude parameters, as defined in Eq. (13-15).

$$\frac{\partial {}^C P}{\partial \Xi} \equiv \begin{bmatrix} \frac{\partial {}^C P}{\partial \Xi_1} & \frac{\partial {}^C P}{\partial \Xi_2} & \frac{\partial {}^C P}{\partial \Xi_3} \end{bmatrix} \tag{12}$$

$$\Xi_1 \equiv \begin{bmatrix} X & Y & Z \end{bmatrix}^T \equiv {}^G P \tag{13}$$

$$\Xi_2 \equiv \begin{bmatrix} X_C & Y_C & Z_C \end{bmatrix}^T \equiv {}^G O_C \tag{14}$$

$$\Xi_3 \equiv \begin{bmatrix} \omega & \phi & \kappa \end{bmatrix}^T \tag{15}$$

The differentiation of ${}^C P$ with respect to Ξ_1, Ξ_2 can be simply expressed as Eq. (16-17).

$$\frac{\partial {}^C P}{\partial \Xi_1} = \frac{\partial {}^C P}{\partial {}^G P} = \frac{\partial\left({}^C_G R({}^G P - {}^G O_C)\right)}{\partial {}^G P} = {}^C_G R \tag{16}$$

$$\frac{\partial {}^C P}{\partial \Xi_2} = \frac{\partial {}^C P}{\partial {}^G O_C} = \frac{\partial\left({}^C_G R({}^G P - {}^G O_C)\right)}{\partial O_C} = -{}^C_G R \tag{17}$$

The differentiation of ${}^C P$ with respect to Ξ_3 is expressed as Eq. (18-19), where R_x, R_y and R_z are the rotation matrix for each axis.

$$\frac{\partial {}^C P}{\partial \Xi_3} = \frac{\partial\left({}^C_G R({}^G P - {}^G O_C)\right)}{\partial \Xi_3} = \begin{bmatrix} \frac{\partial {}^C_G R}{\partial \omega} & \frac{\partial {}^C_G R}{\partial \phi} & \frac{\partial {}^C_G R}{\partial \kappa} \end{bmatrix} ({}^G P - {}^G O_C) \tag{18}$$

$${}^C_G R = R_x(\omega) R_y(\phi) R_z(\kappa) \tag{19}$$

2.3 Mathematical Models with Four Types

The entire linearized mathematical models for BBA is expressed as

$$\begin{bmatrix} y \\ z_1 \\ z_2 \end{bmatrix} = \begin{bmatrix} A_e & A_p \\ K_1 & 0 \\ 0 & K_2 \end{bmatrix}\begin{bmatrix} \xi_e \\ \xi_p \end{bmatrix} + \begin{bmatrix} e_y \\ e_{z1} \\ e_{z2} \end{bmatrix}, \begin{bmatrix} e_y \\ e_{z1} \\ e_{z2} \end{bmatrix} \sim \left(0, \sigma_0^2 \begin{bmatrix} P_y^{-1} & 0 & 0 \\ 0 & P_{Z1}^{-1} & 0 \\ 0 & 0 & P_{Z2}^{-1} \end{bmatrix}\right) \tag{20}$$

where ξ_e and ξ_p are the parameter vectors for the EOP and GP, respectively; y is the observation vector for the tie points;

A_e and A_p are the design matrix derived from the partial differentiation of the collinearity equations corresponding to the tie points with respect to the parameters, ξ_e and ξ_p; z_1 is the observation vector of the EOP provided by the GPS/INS system; z_2 is the observation vector of the GCP provided by the total station and GPS; K_1 and K_2 are the design matrix associated the constraints; e_y, e_{z1} and e_{z2} are the error vectors associated with the corresponding observation vectors; σ_0^2 is the unknown variance component; P_y^{-1} is the cofactor matrix of e_y which is generally expressed as an identity matrix; finally, P_{z1}^{-1} is the cofactor matrix of e_{z1} reflecting the precision of the GPS/INS data and, P_{z2}^{-1} is the cofactor matrix of e_{z2} reflecting the precision of the GCPs.

The mathematical model in Eq. (20) is the most complete one, called Type D in this paper. With the different selections of the subsets of the unknowns and constraints, we can present other three models, Type A-C. In Type A, we estimate only the GPs with the fixed EOPs derived from GPS/INS data without stochastic constraints. In Type B to D, we estimate both GPs and EOPs. As stochastic constraints, we use only GPS/INS data in Type B and only GCPs in Type C. Both kinds of constraints are used in Type D. The main characteristics and mathematical models are summarized in Table 1 and 2, respectively.

	Unknowns to be estimated		Constraints to be used	
	GP	EOP	GPS/INS	GCP
A	O	X	X	X
B	O	O	O	X
C	O	O	X	O
D	O	O	O	O

Table 1. Characteristics of different mathematical models

	Mathematical Models
A	$y = A_p \xi_p + e_y, \ e_y \sim \left(0, \sigma_0^2 P_y^{-1}\right)$
B	$\begin{bmatrix} y \\ z_1 \end{bmatrix} = \begin{bmatrix} A_e & A_p \\ K_1 & 0 \end{bmatrix}\begin{bmatrix} \xi_e \\ \xi_p \end{bmatrix} + \begin{bmatrix} e_y \\ e_{z1} \end{bmatrix}, \begin{bmatrix} e_y \\ e_{z1} \end{bmatrix} \sim \left(0, \sigma_0^2 \begin{bmatrix} P_y^{-1} & 0 \\ 0 & P_{z1}^{-1} \end{bmatrix}\right)$
C	$\begin{bmatrix} y \\ z_2 \end{bmatrix} = \begin{bmatrix} A_e & A_p \\ 0 & K_2 \end{bmatrix}\begin{bmatrix} \xi_e \\ \xi_p \end{bmatrix} + \begin{bmatrix} e_y \\ e_{z2} \end{bmatrix}, \begin{bmatrix} e_y \\ e_{z2} \end{bmatrix} \sim \left(0, \sigma_0^2 \begin{bmatrix} P_y^{-1} & 0 \\ 0 & P_{z2}^{-1} \end{bmatrix}\right)$
D	$\begin{bmatrix} y \\ z_1 \\ z_2 \end{bmatrix} = \begin{bmatrix} A_e & A_p \\ K_1 & 0 \\ 0 & K_2 \end{bmatrix}\begin{bmatrix} \xi_e \\ \xi_p \end{bmatrix} + \begin{bmatrix} e_y \\ e_{z1} \\ e_{z2} \end{bmatrix}, \begin{bmatrix} e_y \\ e_{z1} \\ e_{z2} \end{bmatrix} \sim \left(0, \sigma_0^2 \begin{bmatrix} P_y^{-1} & 0 & 0 \\ 0 & P_{z1}^{-1} & 0 \\ 0 & 0 & P_{z2}^{-1} \end{bmatrix}\right)$

Table 2. Mathematical models of different types

3. EXPERIMENATAL RESULTS

3.1 Data Acquisition

We acquired the experimental data using a GMMS equipped with an omni-directional camera and a GPS/INS system. This camera is actually integrated with six single frame cameras. Its field of view is 360 and 180 in horizontal and vertical direction, respectively. The size of an original image is 1600(H) by 1200(V) pixels while the size of an output integrated image is 5400(H) by 2700(V) pixels. Each pixel covers 1/15 deg in each direction. The specification of

Ladybug, our selected omni-directional camera model, is shown in Figure 2 (Point Grey Research, 2008). The example of omni-directional image captured by the GMMS is shown as Figure 3. We also obtained the position and attitude of the camera when driving along a street using a GPS/INS system. The specification of GPS/INS system is summarized as Table 3 (Appanix, 2009).

Figure 2. Ladybug and GMMS

Figure 3. Example of omni-directional images

X,Y Position Error (m)	0.02
Z Position Error (m)	0.05
Roll and Pitch Error (°)	0.02
True Heading Error (°)	0.05

Table 3. Specification of GPS/INS systems (POS-LV)

3.2 Data Preparation

In this study, we used 24 successive omni-directional images of an area near a road in front of a city hall in a small city, Osan, in Korea. The whole distance between positions of first image and last image is about 100m. The data were obtained by GMMS from east to west side as depicted by the yellow arrow in Figure 4. 13 GPs were measured by a static GPS and total station. Some of them were used as ground control points and the others for ground check points. Figure 5 shows the locations and indexes of ground control points (red) and check points (black). In addition, sufficient number of tie points is manually selected to link the successive images. An example of a pair of tie points is presented in Figure 6.
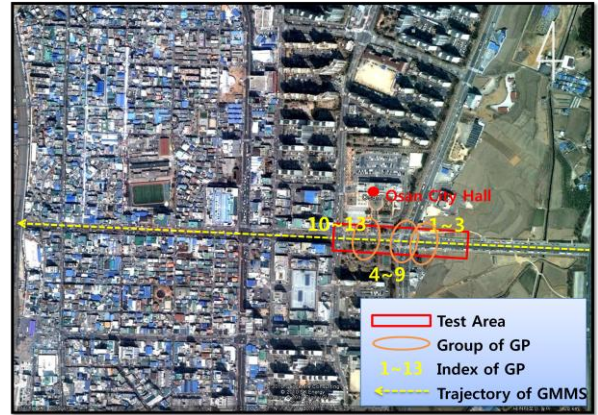

Figure 4. Map of the test area

ID	1, 2, 3	4,5
GPs		

ID	6, 7, 8	9	10, 11, 12, 13
GPs			

Figure 5. Locations of ground control/check points

Image	19th Image	23rd Image
Tie Points		

Figure 6. A pair of tie points

The total number of GPs corresponding to all the tie points is 28. Each GP appears in at least 4 images up to 11 images. The average number of GP overlapped on two successive images is approximately 7.9. The details are summarized in Table 4. The existence of each GP along the images is summarized in Figure 7. The row indexes represent the GP indexes, where the yellow marked indexes indicate the GPs with known coordinates to be used for ground control/check points. The column indexes are the image indexes. Red color indicates the existence of a GP in the corresponding images. For example, the 1st GP exists in the 1st image not in the 2nd image.
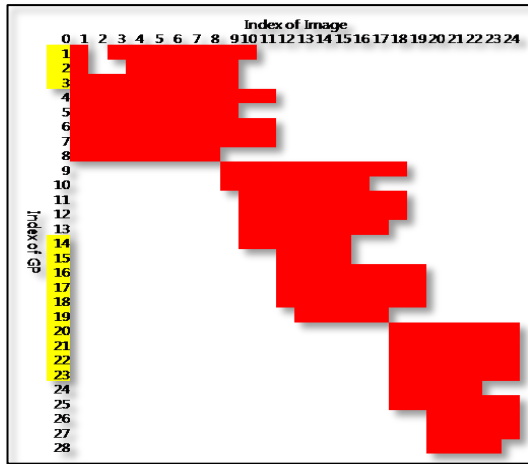
Figure 7. Existence of GPs in images

Parameters	Value
Distance between Images (m)	4
No. Images	24
No. ground control points	4
No. ground check points	9
No. ground points	28
No. image points	212
Avg. no. image per GP	7.6
Avg. no. GP per image	8.8
Avg. no. TP pairs per two successive images	7.9

Table 4. Summary of the experimental data

Finally, we determined the variance-covariance parameters for the mathematical model of BBA. We assumed that the image point measurement error of ±1 deg, the GCP and GPS errors of ±5 cm, and the INS error of ±0.05 deg.

3.3 Result and Analysis

Experiments have been conducted with real data for the evaluation of the proposed BBA method with the mathematical models of four different types. The GPs estimated from BBA were compared with those measured by a statics GPS and a total station. The GP errors from this comparison are described in Table 5.

The RMSE from Type B using only EOP constraints is not improved even in comparison with that from Type A using no constraint with fixed EOPs. This means that the EOPs estimated in Type B are almost the same as the EOPs initially provided from GPS/INS data, used as fixed EOPs in Type A. This must be caused from the assumption of the significantly larger errors in image point measurement comparing to the GPS/INS errors. Hence, the relative orientation determined from TPs cannot improve the EOP provided from GPS/INS data.

In Type C, we performed the BBA with only 4 GCPs (ID 1, 4, 8 and 10) without any EOP constraints. The RMSE of type C is significantly reduced comparing with the errors from other types. We can determine GPs with a RMSE of less than ±5 cm. According to this result, GPs can be estimated very accurately with a small number of GCPs. To use Type C, however, some GCPs have to be measured accurately in advance. For Type D, we use 4 GCPs and EOP constraints. The RMSE is reduced slightly comparing with Type A and B, but not large enough when comparing with Type C.

According to the test results, we can infer that EOPs contain systematic bias, and it could be propagated from the difference between the GPS/INS coordinate system and CCS. In future, the conformal transformation parameters between the two coordinate systems will be estimated simultaneously during the BBA process.

The residuals between the measured image points (IPs) and adjusted IPs are shown in Figure 8 for all four types. Large residuals indicate the large difference between the measured

ID	Type A : No Constraints and Fixed EOP			Type B : Only EOP Constraints			Type C : Only GCP Constraints			Type D : Both EOP and GCP Constraints		
	ΔX	ΔY	ΔX	ΔY	ΔZ	ΔZ	ΔY	ΔZ	ΔZ	ΔX	ΔY	ΔZ
1	-0.334	-0.055	-0.734	-0.337	-0.036	-0.759	0.000	0.000	0.000	-0.140	-0.042	-0.289
2	-0.401	-0.137	-0.683	-0.387	-0.122	-0.704	0.019	-0.042	0.019	-0.370	-0.116	-0.658
3	-0.253	-0.169	-0.567	-0.261	-0.148	-0.600	0.020	-0.015	0.036	-0.213	-0.125	-0.545
4	-0.538	-0.481	-0.840	-0.542	-0.455	-0.824	0.000	0.000	-0.001	-0.049	-0.025	-0.073
5	-0.551	-0.289	-0.901	-0.557	-0.261	-0.883	0.003	-0.012	-0.019	-0.541	-0.257	-0.857
6	-0.315	-0.482	-0.931	-0.301	-0.505	-0.936	-0.013	0.003	0.050	-0.253	-0.516	-0.904
7	-0.349	-0.441	-0.926	-0.338	-0.463	-0.930	-0.023	0.048	0.056	-0.290	-0.475	-0.898
8	-0.302	-0.491	-0.956	-0.289	-0.514	-0.959	0.000	0.000	0.001	-0.106	-0.052	-0.184
9	-0.290	-0.201	-0.571	-0.290	-0.210	-0.569	0.082	-0.044	0.130	-0.277	-0.199	-0.544
10	-0.236	-0.442	-0.742	-0.248	-0.439	-0.768	0.000	0.000	0.000	-0.052	-0.109	-0.184
11	-0.238	-0.444	-0.739	-0.251	-0.442	-0.765	-0.015	-0.001	0.001	-0.202	-0.441	-0.709
12	-0.234	-0.434	-0.735	-0.241	-0.438	-0.761	0.011	-0.015	-0.004	-0.197	-0.432	-0.704
13	-0.250	-0.417	-0.737	-0.257	-0.420	-0.762	0.006	0.000	-0.005	-0.214	-0.416	-0.705
AVG	-0.330	-0.345	-0.774	-0.331	-0.342	-0.786	0.007	-0.006	0.020	-0.223	-0.247	-0.558
STD	0.103	0.148	0.124	0.102	0.157	0.116	0.025	0.022	0.038	0.128	0.177	0.276
RMSE	0.360	0.390	0.816	0.360	0.392	0.827	0.027	0.024	0.045	0.268	0.316	0.648

Table 5. Comparison of GP errors for Type A-D (unit: m)

and adjusted IPs, and EOPs or GCPs may not be estimated accurately. According to the statistics of residual for 4 types shown in Table 6, the RMS value of the residuals from Type C are remarkably small in comparison with those from other types. This indicates that the mathematical model of Type C is the most accurate. Estimated GPs, EOPs and GCPs for Type D are shown in Figure 9, where the blue points are the estimated GPs; the red points are the estimated EOPs; the red circle are ground control points; the green circle is the ground check points.
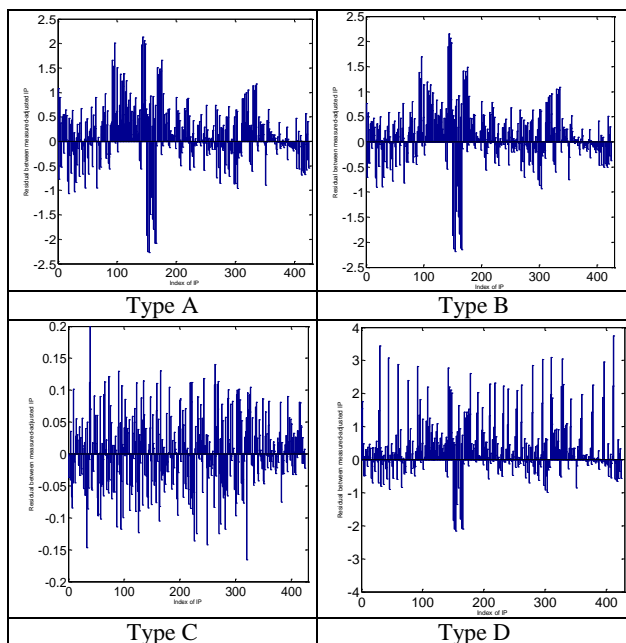

Figure 8. Residuals between measured and adjusted IPs

Type	Min	Max	AVG	STD	RMS
A	-2.270	2.136	0.142	0.600	0.616
B	-2.181	2.152	0.117	0.539	0.551
C	-0.166	0.203	0.003	0.056	0.057
D	-2.157	3.752	0.350	0.843	0.912

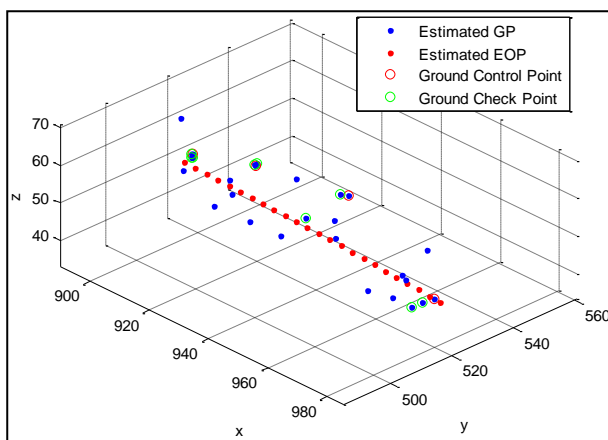Table 6. Statistics on residuals

Figure 9. Plot of EOPs (projection centers), GPs and GCPs

4. CONCLUSIONS

In this paper, we developed a BBA method for omni-directional images obtained from a ground mobile mapping system. We derived new collinearity equations for omni-directional images and proposed the mathematical models with four types for BBA. The proposed method has been tested with real urban data and could successfully estimate GPs using a small number of GCPs with a RMSE of less than ±5cm. This study shows that we can accurately determine EOPs and GPs from omni-directional images with the accuracy level required for precision road-side 3D mapping. Furthermore, this study will be efficiently utilized to generate more realistic street view and 3D urban modelling. In future, we plan to perform more sophisticated lens calibration for the omni-directional camera to improve the georeferencing accuracy of the omni-directional images.

REFERENCES

Aizawa, K., 2004. *Image processing technologies: algorithms, sensors, and applications*, Signal Processing and Communications Series, New York, pp. 116-117.

Applanix, 2009. "POSLV specifications", Applanix Inc., Canada, http://applanix.com/products/land/pos-lv.html (accessed 4 Mar. 2010)

Beauchemin, S. S., 2001. Modeling and removing radial and tangential distortions in spherical lenses, In: *Multi-Image Analysis, Lecture Notes in Computer Science*, vol. 2032, pp. 1–21.

Choi, K., 2009. Image georeferencing using at without GCPs for a UAV-based low-cost multisensor system. *Korean Society of Surveying, Geodesy, phtogrammetry, and Cartography*, 27(2),pp. 249-260.

Gontran, H., 2003. A mobile mapping system for road data capture via a single camera, In: *Proceedings of the Optical 3D Conference*, Zurich, Switzerland,.

Point Grey Research, 2008. "Ladybug specifications", Point Grey Research Inc., Canada, http://www.ptgrey.com/products/spherical.asp (accessed 6 Apr. 2010)

Silpa-Anan. C., 2005. Visual localization and loopback detection with a high resolution omnidirectional camera, *Proceedings of the Omnivis workshop,* Workshop on Omnidirectional Vision.

Tao, V. C., 2005. Mobile mapping technology for road network data acquisition, *Proc. Journal of Geospatial Engineering*, 2(2), pp.1-13.